Highly effective clean-up of magnetic nanoparticles using microfluidic technology

V. F. Cardoso,[a,b] D. Miranda,[a] G. Botelho[c], G. Minas[b] and S. Lanceros-Méndez[a,d,e]

[a]Centro/Departamento de Física, Universidade do Minho, Campus de Gualtar, 4710-057 Braga, Portugal. Email: vanessa@dei.uminho.pt

[b]CMEMS-UMinho, Universidade do Minho, DEI, Campus de Azurém, Guimarães 4800-058, Portugal

[c]Centro/Departamento de Química, Universidade do Minho, Campus de Gualtar, 4710-057 Braga, Portugal

[d]BCMaterials, Parque Científico y Tecnológico de Bizkaia, 48160-Derio, Spain.

[e]IKERBASQUE, Basque Foundation for Science, 4803, Bilbao, Spain

The successful application of magnetic nanoparticles (MN) is highly dependent of their effective cleaning after synthesis and/or before their use in order to remove solvents, excess of surfactant, byproducts and undesired impurities that can be toxic and/or cause side effects, hindering their applicability. As manual cleaning is a time consuming and inefficient process, this work introduces the design, fabrication and testing of a simple microfluidic system able to continuously clean and separate MN. The geometrical configuration of the microfluidic channels and the experimental conditions are first optimized using finite element simulations. Next, the system is tested for the cleaning and the separation of iron oxide nanoparticles synthesized by coprecipitation. Cleaning efficiency of about 99.7 % is obtained controlling the fluid flows in the microfluidic system with residual loss of magnetic nanoparticles, demonstrating the potential of this technology for the cleaning and the separation of magnetic entities.

Keywords: magnetic nanoparticles, cleaning, manipulation, microfluidic

1 Introduction

Magnetic nanoparticles (MN) are being intensively developed and applied in a wide range of biomedical applications including site-specific drug delivery systems, contrast agents in magnetic resonance imaging, cancer thermotherapy, biosensing and bioseparation, among others [1-3]. MN allow the possibility of being remotely manipulated or generating thermal energy in response to an external magnetic field [4] Their shape and size are easily controllable and can range from a few up to tens of nanometers [5]. This small scale provides a high hydrothermal stability, improved tissular diffusion and a large surface area to volume ratio that increases the available area for chemical binding/adsorption and, consequently, target/analyte capture efficiency [6-7]. Therefore, in some applications MN are coated or grafted with biological or chemical entities not only to avoid oxidation and guaranty nontoxicity, but also to functionalize the nanoparticles in order to provide a controllable way for the tagging/binding of drugs, proteins, enzymes, antibodies or nucleotides, which is at the basis of the aforementioned biomedical applications [8-10].

The selection of the magnetic core and respective functionalization is application-specific in order to achieve optimized performance of the nanocomposite. Although nickel and cobalt are highly magnetic responsive materials, their use in biomedical applications is limited due to their toxicity and susceptibility to oxidation [6]. Therefore, superparamagnetic iron oxide nanoparticles (SPIONS) such as magnetite (Fe_3O_4) or maghemite (γ-Fe_2O_3) are by far the most commonly magnetic cores employed in the biomedical field because of their manufacture simplicity, high saturation magnetization and for not retaining any magnetism after removal of the magnetic field [11-12]. A number of methods have been

developed to synthesize SPIONS, including ultrasound radiation, laser ablation, mechanical grinding, sol-gel, thermal decomposition and coprecipitation [13-15]. These last two methods are the most commonly used and both allow synthesizing SPIONS with optimized particle size and shape, size distribution, surface chemistry and magnetic properties [6]. Together with other physicochemical parameters, the successful application of such materials is highly dependent on their effective cleaning after synthesis and/or before their use in order to remove the used solvents, the excess of surfactants, the byproducts and/or the undesired impurities, which can be toxic and/or cause side effects in specific applications. The cleaning process of synthesized (and eventually coated/functionalized) MN is usually performed by multi-step procedures involving filtrations, centrifugations or manually with the help of a powerful magnet [16-17]. In both cases, MN are repeatedly cleaned (at least three times) using for example water, ethanol and/or acetone [14, 18]. Together with being time consuming, a large amount of nanoparticles are often lost and traces of solvents, surfactants or byproducts still remain after the process. In order to overcome these limitations, microfluidic technology appears as an interesting and powerful alternative method for the automated and continuous cleaning and separation of the MN. Currently, the fast and accurate manipulation of particles in microfluidic systems can be carried out by a variety of methods using active techniques such as magnetic, acoustic, dielectrophoresis (DEP); passive techniques such as pinched flow fractionation (PFF), microvortex manipulation, deterministic lateral displacement; or a combination of them [19]. It is to notice that active techniques that make use of external fields offer better performance than passive techniques that relies on the interaction between particles, flow field and channel structure.

In this scope, the specific case of magnetic manipulation has gained increasing importance in many research fields involving magnetic particles and magnetically labeled biological compound [20-23], since magnetic sorting can be carried out at high-throughput in virtually any biological or chemical fluids with high specificity, minimal power requirements and without damaging the sorted compound [24-25]. Most of these applications are miniaturized versions of pre-existing large scale procedures, although with the added advantage of favorable scaling down dimensions, which include portability, low reagent consumption, fast analysis time and low cost [26-27]. To the best of our knowledge, no microfluidic system has been yet optimized and tested for the automated, continuous and effective cleaning and separation of synthesized MN, which is, as referred previously, an imperative procedure before their coating, functionalization, use or re-use. Thus, the system presented in this work explores: the laminar nature of flow that allows the continuous movement of layers of different fluids within microchannels [28] and (2) magnetic forces that are able to deflect MN from one flow to another adjacent flow, as illustrated in Figure 1. In the case of the concerned application, Fluid B represents the synthesis solution together with the MN injected into the Inlet B, while Fluid A corresponds to the cleaning solution injected into the Inlet A.

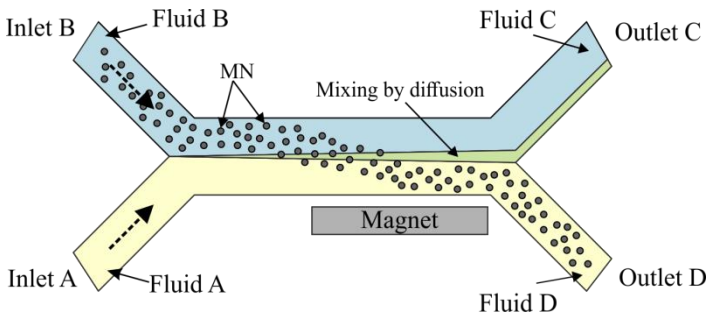

Figure 1. Schematic representation of continuous cleaning and separation of MN in a microfluidic system.

Finite element analysis models were first developed to optimize the geometrical configuration and experimental conditions of the microfluidic system, in order to control the diffusion on the fluids interface along the microchannel and maximize the purity of the cleaning solution (Fluid D) exiting at the outlet D where the MN are collected. On the other hand, it is intended that Fluid C composed by the synthesis solution and the diffusion solution, which will be called waste, exit at the Outlet C represented in Figure 1. According to the results, a polydimethylsiloxane (PDMS) microfluidic system was then fabricated by soft lithography and tested for the continuous cleaning and separation of SPIONS synthesized by coprecipitation. An optical microscope was used to visualize the deflection of the SPIONS under magnetic field and gas chromatography technique was used to analyze the solution on each outlet in order to determine the cleaning efficiency of the system.

2 Simulations of the system geometry and flows

Finite element simulations were performed in order to study the diffusion behavior of the fluids within the microchannel since it has a direct influence on the cleaning efficiency of the system and therefore optimize the geometrical configuration of the microfluidic system as well as the flow rates, accordingly. Two dimensional (2D) simulations were carried out, using COMSOL Multiphysics, version 5.2a, as they show proper characteristics for the optimization process of the system [29].

2.1 Model and governing equations

Fluids flow, which is assumed incompressible, is described by the Navier-Stokes equations. Additionally, due to the small dimensions and typically low volumetric flow, fluid handling within microchannels is restricted to the laminar regime,

with Reynolds numbers (Re) typically lower than 10 [30]. Under these conditions the unsteady inertial force dominates over the non-linear inertial force [31]. Moreover, the convective mass transfer between the fluids occurs only by diffusion in the flow direction and so, Flick's law was used to explain this behaviour [32-33]. Table 1 shows the main equations governing the phenomena occurring within the microfluidic system.

Table 1. Summary of the fundamental equations governing the different processes involved in the microfluidic channel model [33].

Physical process	**Governing Equation**
Navier-Stokes	$\rho_i.\left(\frac{\partial v_i}{\partial_t} + v_i.\nabla v_i\right) = -\nabla p + \mu_i.\nabla^2 v_i$
Incompressible flow	$\nabla.(\rho_i v_i) = 0$
Flick's law	$\frac{\partial c_i}{\partial_t} + v_i.\nabla \mathrm{c_i} = \mathrm{D}.\nabla^2 \mathrm{c_i}$
Reynolds number	$R_e = \frac{\rho_i.v_i.L}{\mu_i}$

The variables ρ_i, v_i, $\mathrm{c_i}$ and μ_i correspond to fluid density, fluid velocity, concentration of species within the fluid, and fluid viscosity, respectively. Subscript $_i$ concerns to the fluid itself, and it is identified as *A*, *B*, C and *D*, where *A* and *B* correspond to the fluids injected into the Inlets A and B and *C* and *D* represent the fluids that exit through the Outlets C and D (Figure 1). The variables t, p, L are the time, pressure and length of the diffusion microchannel, respectively.

2.2 Boundary conditions

The boundary conditions defined accordingly to the Navier-Stokes and Flick's law equations are schematically presented and defined in Table 2. The boundary conditions 1 and 2 correspond to the inflows of Fluids in Inlets A and B, respectively, where the flow rates (Q_A and Q_B) and the initial concentrations ($c_{A,0}$ and $c_{B,0}$) are defined. The boundary conditions 3 and 4 correspond to the outflows in each outlet C and D, where a

null initial pressure value was admitted to represent free flow. The diffusion of species between Fluids A and B are represented by the boundary condition 5. Finally, the non slip boundary condition is applied to all the microfluidic channel walls (boundary 6).

Table 2. Summary of the boundary conditions implemented in the microfluidic model.

Schematic representation of the boundary conditions			
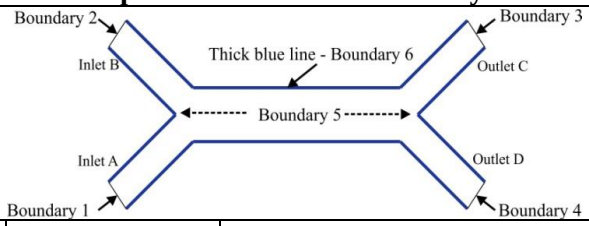			
Boundaries	**Boundary type**	**Boundary condition**	**Model**
Boundary 1	Inlet	Laminar inflow with flow rate, Q_A	Navier-Stokes
Boundary 2	Inlet	Laminar inflow with flow rate, Q_B	
Boundaries 3 and 4	Outlet	Pressure, Suppress backflow, p_0=0 Pa	
Boundary 6	Wall	No slip	
Boundary 1	Fluid A - Inlet	Initial concentration of species, $c_{A,0}$	Flick's Law
Boundary 2	Fluid B - Inlet	Initial concentration of species, $c_{B,0}$	
Boundaries 3 and 4	Outflow	$-n.D_i.\nabla c_i = 0$	
Boundaries 6	Flux	No Flux – apply for all species	
Boundary 5	Diffusion	Diffusion, D	

2.3 Numerical simulations results

The diffusion behavior of the fluids along the microchannels was evaluated by considering the effect of the different parameters of the microfluidic model. The system was tested using alkaline solvents, such as ammonium hydroxide, commonly used as catalyst for the synthesis of SPIONS, and cleaning solvents such as water, ethanol or acetone. Further, different configurations and dimensions of the microfluidic channels as well as different fluids flows were evaluated. Due to the similarity of the obtained data, only the simulations with ammonium hydroxide solution (NH_4OH, 28-30 % w/w)

and water are presented, being representative for the other solutions. These solutions correspond to those used in the experimental study. It is to notice that in the theoretical model Fluid B was defined as pure NH_4OH, which is an approximation to the real synthesis solution of SPIONS that involves a mixture of NH_4OH and water. The values of the parameters used in the numerical simulations can be found in Table 3. In order to study the diffusion between fluids, the concentration of Fluid A in Inlet A was defined as 100 $mol.m^{-3}$, while the concentration of Fluid A in Inlet B was defined as 0 $mol.m^{-3}$.

Table 3. Parameters and values used in the numerical simulation of the microfluidic system.

Parameter	Designation	Unit	Value
ρ_A	Density of Fluid A	$kg.m^{-3}$	997
ρ_B	Density of Fluid B	$kg.m^{-3}$	910
Q_A	Flow of Fluid A	$\mu L.min^{-1}$	5, 15, 25, 50, 75 and 100
Q_B	Flow of Fluid B	$\mu L.min^{-1}$	5, 15, 25, 50, 75 and 100
T	Temperature	K	298
μ_A	Viscosity of Fluid A	Pa.s	8.94×10^{-3}
μ_B	Viscosity of Fluid B	Pa.s	1.38×10^{-4}
p_0	Pressure	Pa	0
D	Diffusion coefficient of species	$m^2.s^{-1}$	1×10^{-11}
$c_{A,0}$	Concentration of Fluid A in Inlet A	$mol.m^{-3}$	100
$c_{B,0}$	Concentration of Fluid A in Inlet B	$mol.m^{-3}$	0

Preliminary results demonstrated the suitability of the microfluidic system geometry schematically represented in Figure 2.

Figure 2. Schematic representation of the optimized microfluidic system. Fluid A: cleaning solution; Fluid B: synthesis solution; Fluid C: waste; Fluid D: cleaning solution. Channel widths (a) 600 µm; (b) 400 µm; (c) 600 µm; (d) 400 µm; diffusion channel length (e) 10 mm.

The Inlet A, where the cleaning solution (Fluid A) is introduced, features a width of 600 µm, which is 1.5 times the one of Inlet B, where the synthesis solution (Fluid B) is introduced. In turn, the width of the Outlet D, where the cleaning solution exits (Fluid D) is of 400 µm, half the one of the Outlet C where the waste fluid (Fluid C) exits. The width and length of the diffusion path are 1 mm and 10 mm, respectively.

The concentration profiles of the fluids inside the microfluidic system obtained from the numerical simulations are presented in Figure 3. In this case, the flow rate of the synthesis solution (Q_B) is kept constant at 50 µL.min^{-1} while the flow rate of the cleaning solution (Q_A) ranges between 5 and 100 µL.min^{-1}. These values enable a balance between the hydrodynamic and magnetic forces ensuring the deflection of the MN from the synthesis solution to the cleaning solution, observation not considered in this simulation but tested experimentally. The pure cleaning solution (Fluid A) at Inlet A was set as a concentration, $c_{A,0}$, of 100 mol.m^{-3} and is identified with a deep red color, while its concentration, $c_{B,0}$, at Inlet B was set to be 0 mol.m^{-3}, and depicted in a deep blue color. At this stage it is important to remember that the final purpose of the microfluidic system is that the waste fluid composed by the synthesis solution along with the diffusion solution, byproducts of the synthesis and undesired impurities leave at the Outlet C and that the cleaning solution along with the MN, which are deflected from one solution to another solution by the application of a magnetic force, leave at the Outlet D.

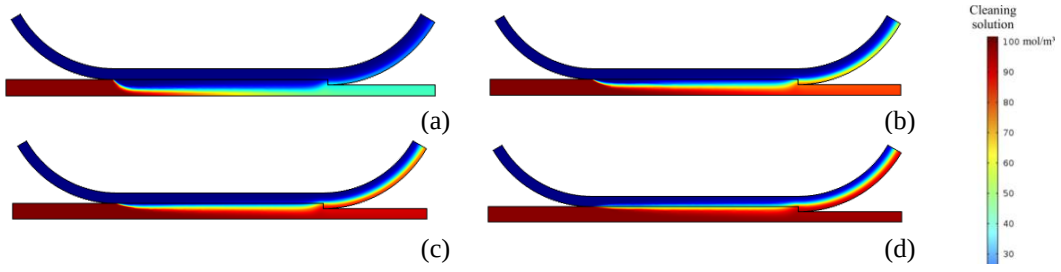

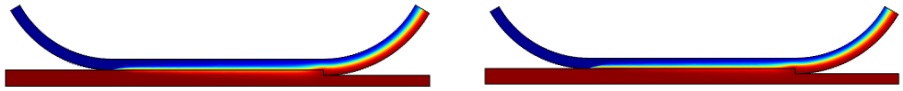

(e) (f)

Figure 3. Concentration profiles of the fluids inside the microfluidic channel for a synthesis solution flow rate, Q_B, of 50 µL.min^{-1} and cleaning solution flow, Q_A, of 5 µL.min^{-1}; (b) 15 µL.min^{-1}; (c) 25 µL.min^{-1} ; (d) 50 µL.min^{-1}; (e) 75 µL.min^{-1} and (f) 100 µL.min^{-1}. Colour bar: the deep red and blue colours correspond to 100 and 0 mol.m^{-3}concentration of cleaning solution (Fluid A), respectively. The intermediate colours correspond to the relative cleaning solution content.

The results demonstrate that the ratio between the flow rate of both fluids has a significant effect on the diffusion behavior along the microchannel. The higher the cleaning solution flow rate, higher is also its concentration in Outlet D, which can be observed by the increase of the red color in this section of the microfluidic system, especially for flows equal or higher than 50 µL.min^{-1} (Figure 3d, 3e and 3f). These results can be analyzed in more details in Figure 4a that represents the concentration of the cleaning solution, c_A, in the microchannel cross section at the end of the 10 mm diffusion path and entries to the Outlet C and D (see y-axis at Figure 2). Figure 4b illustrates the concentration of the cleaning solution c_A in the Outlet D for various Q_A and Q_B. In practical terms, c_A equals the percentage of cleaning solution, i.e. water, that exits though each outlet and high values closer to 100 mol.m^{-1} are expected at the Outlet D.

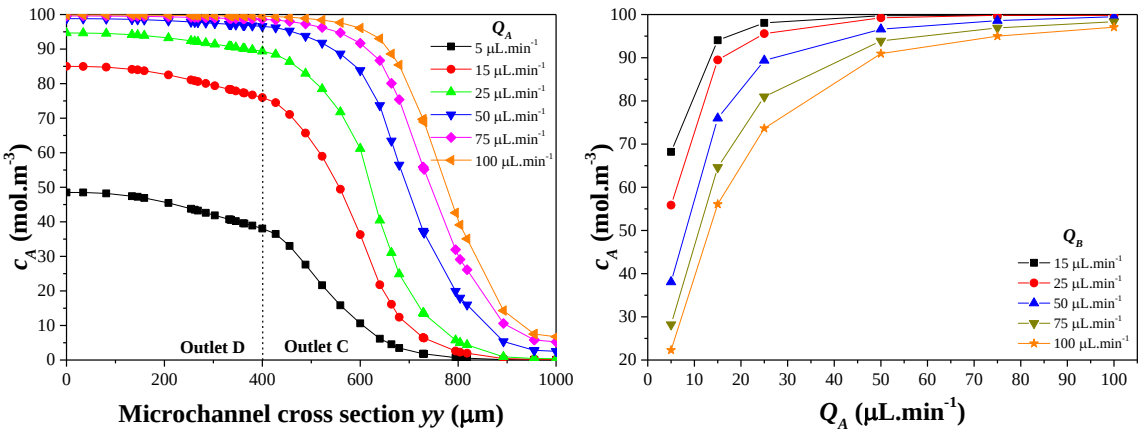

(a) (b)

Figure 4. Concentration of the cleaning solution, c_A, (a) at the entries of Outlet C and D (see y-axis at Figure 2), maintaining the synthesis fluid flow, Q_B, at 50 µL.min^{-1} and (b) in the Outlet D varying Q_A and Q_B.

Maintaining Q_B, at 50 µL.min^{-1} and varying Q_A at 50, 75 and 100 µL.min^{-1}, c_A of 96.6, 98.6 and 99.5 mol.m^{-3} are obtained at the Outlet D, respectively. Moreover, the results presented in Figure 4b allow concluding that higher values of c_A are obtained when Q_A is equal or higher than Q_B. The extremely high concentration of cleaning solution that can be obtained at Outlet D by properly controlling the channel geometry and fluids flows demonstrates the potential of the microfluidic system for the cleaning of MN. Thus, the next step was the fabrication of the PDMS microfluidic system (see Experimental Section for the microfluidic system fabrication) and the experimental evaluation of the system efficiency for the automated and continuous cleaning and separation of synthesized magnetic iron oxide nanoparticles (see Experimental Section for the iron oxide synthesis procedure).

3 Fabrication and evaluation of the microfluidic system

3.1 Fabrication of the microfluidic system

For the fabrication of the microfluidic system, SU-8 100 (epoxy-based negative photoresist) and Sylgard® 184 Silicone Elastomer (PDMS) were obtained from Microchem and Dow Corning, respectively, and isopropyl alcohol (IPA) was supplied from Sigma-Aldrich.

The PDMS microfluidic system was fabricated by replica molding using a prefabricated SU-8 mold obtained through a low cost photolithography process. The SU-8 mold features a thickness of 250 µm and geometry and dimensions according to Figure 2. Details on the processing steps and parameters used for the fabrication of the SU-8 mold can be found in [34]. The processing conditions are summarized in Table 4.

Table 4. Processing conditions used to obtain the SU-8 mold [34].

Conditions/SU-8 thickness (µm)		250
Substrate (mm)		Glass slides (26x76)
Rotational speed (rpm)		2100
Pre-bake time (min)	at 65 ºC	35
	at 95 ºC	70
UV exposure time (min)		9
Post-bake time (min)	at 65 ºC	10
	at 95 ºC	15
Development time (min)		20

In short, SU-8 100 was deposited on a cleaned glass slide (26×76 mm) using a spin-coater (Polos 2000) at a rotational speed of 500 rpm, acceleration of 300 rpm.s^{-1} during 7 s followed by a rotational speed of 2100 rpm, acceleration of 300 rpm.s^{-1} during 30 s, in order to obtain a thickness of 250 µm at the end of the fabrication process. Then, the sample was subjected to a pre-bake step at 65 ºC and 95 ºC using a hot-plate (*Prazitherm* type *PZ23-2*, 1400W) at a heating rate of 20 Watt% as described in Table 4. After UV exposure at 350 nm for 9 min (*Photomeca- type IPP 45*) using a previously impressed patterned photolitho, the sample was subjected to a post-bake step and immersed in SU-8 developer for 20 min in order to remove the non-exposed epoxy. Finally, the sample was properly cleaned with IPA and dried gently with compressed air in order to obtain the final SU-8 mold.

In order to obtain the PDMS microfluidic system, a PDMS solution composed of 5:1 %wt of base:curing agent was prepared and placed in a home-made vacuum system for air bubbles removing. The solution was deposited slowly on the SU-8 mold surrounded by aluminum adhesive tape. Simultaneously, another PDMS solution composed of 20:1 %wt of base:curing agent was prepared, placed in the vacuum system and deposited in a cleaned glass slide (26×76 mm) by spin-coating at a rotational speed of 3000 rpm, acceleration of 300 rpm.s^{-1} during 50 s. The PDMS microchannel and the PDMS glass slide were left to cure partially at 80 ºC for 20 min. After opening the inlets

and outlets, the PDMS microchannel was bonded irreversibly to the PDMS glass slide by curing completely at 80 ºC for 2 h. A photograph of the final PMDS microfluidic system is presented in Figure 5a.

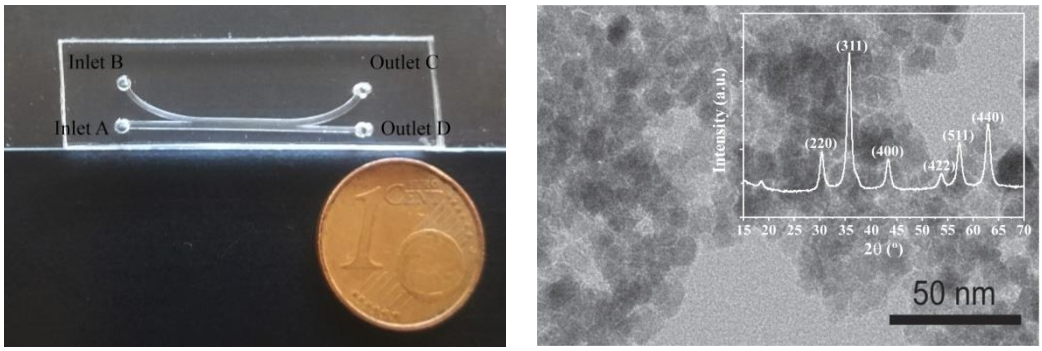

(a) (b)

Figure 5. (a) Photograph of the PDMS microfluidic system; (b) TEM image of the SPIONS used to test the cleaning efficiency of the PDMS microfluidic system with the corresponding XRD spectrum as inset.

Prior to each experiment, the PDMS microchannel was flushed with NaOH (0.5 M) and water, followed by 1 % of bovine serum albumin (BSA) solution during 30 min, both acquired from Sigma-Aldrich. This step is essential to avoid the deposition of MN on the walls of the microchannel.

3.2 Synthesis of the magnetic iron oxide nanoparticles

The efficiency of the microfluidic system for the cleaning and separation of MN was tested using SPIONS synthesized by coprecipitation in air atmosphere and at room temperature adapting our previous work [35]. All compounds were supplied by Sigma-Aldrich. Ultrapure and deionized water were prepared in the laboratory. Briefly, 5 mL of ammonium hydroxide solution (NH_4OH, 28-30 % w/w) was added drop by drop to 5 mL of an aqueous mixture of iron (II) chloride tetrahydrate ($FeCl_2.4H_2O$) and iron (III) chloride hexahydrate ($FeCl_3.6H_2O$) with a Fe^{2+}/Fe^{3+} molar ratio of 2/3, under vigorous stirring. The solution was kept under mechanical stirring for 30 min. Due to the high concentration of the MN synthesized and in order to allow their easier cleaning

without causing blockage of the microchannels, the solution was diluted by adding 10 mL of water. Then, half of the MN in solution was cleaned manually six times with water using a strong magnet. The rest of the MN in solution was cleaned using the microfluidic system.

Through this synthesis, superparamagnetite Fe_3O_4 nanoparticles were obtained with an average diameter of 10±1.7 nm, normalized magnetization of 67 emu.g^{-1} at 10 kOe and coercivity of 1.6 Oe [35]. A TEM image (Tecnai T20, from FEI) of the SPIONS is presented in Figure 5b. Further, the corresponding X-ray diffaction (XRD) spectrum (*Bruker D8 Discover* diffractometer using Cu Kα incident radiation) in shown as inset.

3.3 Evaluation of the microfluidic system cleaning efficiency

The experimental setup used to test the PDMS microfluidic system is illustrated in Figure 6. The setup is composed by an inverted microscope *Olympus CKX41* (Figure 6a *i*) equipped with a high speed camera *Olympus I-SPEED LD* (Figure 6a *ii*) that allows to visualize the flow of the SPIONS inside the microfluidic system. The fluid flow was controlled using a syringe pumps system from *neMESYS* (Figure 6a *iii*) and the *neMESYS* user interface (Figure 6a *iv*). A closer view of the PDMS microfluidic system placed in the microscope is presented in Figure 6b.

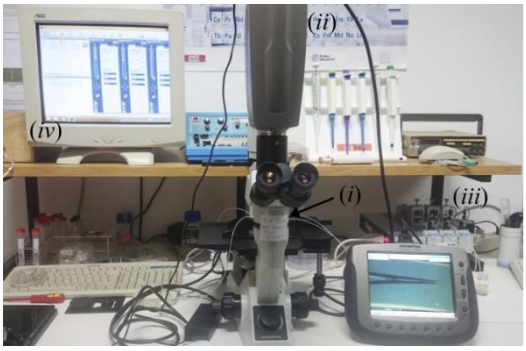

(a)

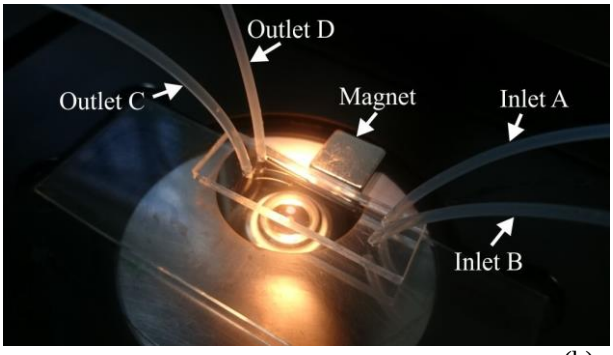

(b)

Figure 6. Photographs of (a) experimental setup: (*i*) inverted microscope; (*ii*) high speed camera; (*iii*) syringe pumps; (*iv*) syringe pump user interface and (b) PDMS microfluidic channel mounted in the microscope.

After the proper functionalization of the microfluidic system and in order to evaluate the simulated results presented in Figure 4a, the synthesis solution with the SPIONS was flushed into Inlet B maintaining Q_B at 50 µL.min^{-1} and the cleaning solution composed of ultrapure water was flushed into Inlet A with Q_A varying from 5 to 100 µL.min^{-1}. The manipulation of the SPIONS inside the microfluidic system under magnetic forces is illustrated in Figure 7. Without magnetic force (Figure 7a), the SPIONS flow in the upper section of the microfluidic channel along with the synthesis solution and exit though the Outlet C. Using a commercial neodymium magnet (*Q-10-10-01-N* from *Supermagnete*) positioned near the microfluidic channel (at 9 mm from the Inlet A and 2 mm from the microchannel, Figure 6b), the SPIONS were deflected from the upper to the lower solution in order to continuously exist through the Outlet D, along with the cleaning solution (Figure 7b). Changing the relative position of the magnet and the microchannel will lead to a modification of the magnetic interactions and to a decrease of the separation efficiency. The visualization of SPIONS in the microfluidic system with this setup was possible due to the formation of some aggregates during the process. Further, after each experiment, a stronger neodymium magnet (*Q-40-20-10-N* from *Supermagnete*) was used to separate the SPIONS from the solutions in each outlet in order to confirm their efficient deflection.

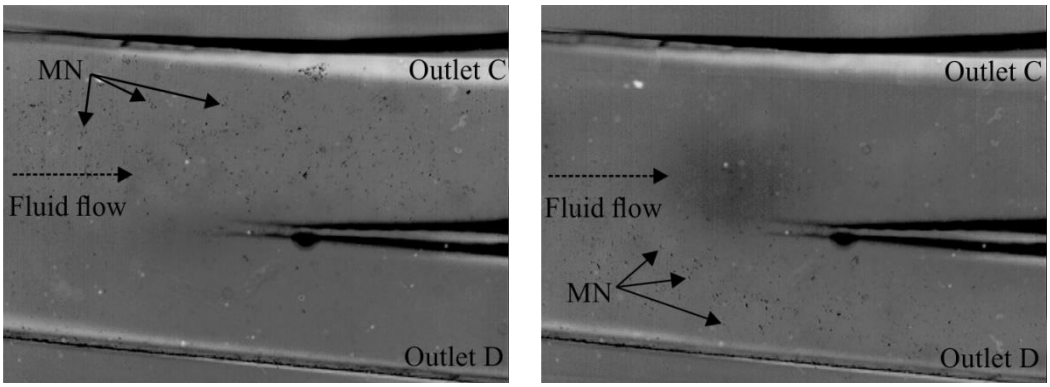

Figure 7. Photographs of the microfluidic system with the position of the SPIONS at the entries of the Outlets C and D with a Q_A of 75 µL.min^{-1} (a) without and; (b) with applied magnetic force.

After the deflection of the SPIONS within the microfluidic channel, gas chromatography was used to analyze the solutions leaving Outlet D and therefore to determine the cleaning efficiency of the microfluidic system as a function of Q_A. A gas chromatograph *Chrompack CP 9000* with flame ionization detector at 200 ºC and injector at 150 ºC was used. The stationary phase was a packed column Carbowax 20 M 10 % in Chromosorb WHP (3 m length and 2 mm internal diameter) starting from room temperature till 110 ºC using an heating rate of 10 ºC.min^{-1} and the mobile phase was a flow of nitrogen at 70 kPa. Before each experiment, the solution was separated magnetically from the SPIONS. Three measurements were performed in each case, also for the solution obtained after manual cleaning. Since water cannot be detected, the cleaning efficiencies were calculated indirectly by the decrease of the NH_4OH peak area (which is proportional to its concentration) in the Outlet D comparatively to the initial dilute synthesis solution used and flushed into the Inlet B. The results obtained theoretically and experimentally are presented in Figure 8.

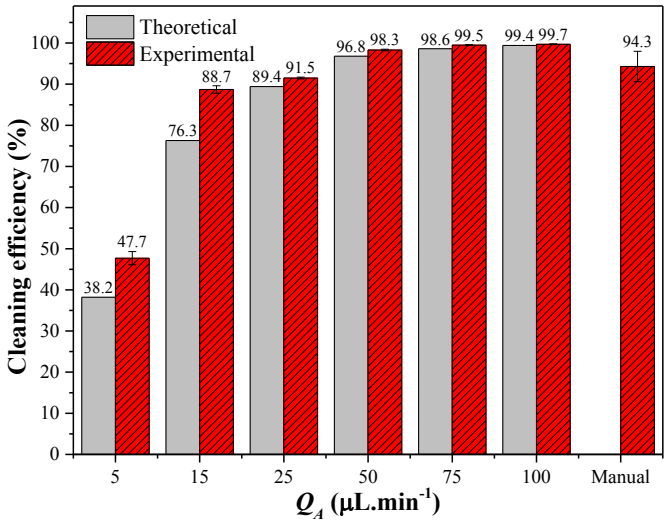

Figure 8. Theoretical and experimental cleaning efficiencies of the synthesized SPIONS using the optimized PDMS microfluidic system maintaining Q_B at 50 µL.min^{-1} and varying Q_A from 5 to 100 µL.min^{-1} and manually with the aid of a strong magnet.

The experimental results of the cleaning efficiencies showed values near but larger than the theoretical results. This phenomenon is justified by the dilution process of the synthesis solution that was performed before the cleaning process that automatically increased the concentration of water, c_A. For Q_A equal or higher than Q_B, i.e. 50 µL.min^{-1}, cleaning efficiencies higher than 98 % were obtained. More precisely, for Q_A of 75 and 100 µL.min^{-1}, cleaning efficiencies of 99.5 and 99.7 % were reached, respectively, which are superior to the 94.3 % obtained manually that depend on the ability of the scientist and show, consequently, higher standard deviation. It should be noted that some residual NH_4OH or impurities can remains within the SPIONS agglomerates both in manual and microfluidic cleanings. Nevertheless, although not measured, a larger amount of NH_4OH or impurities should be expected in the manual cleaning due to the nanoparticles collection procedure (by using a magnet or by centrifugation) that increases the formation of agglomerates and makes difficult further dispersion within the cleaning solution for additional washes. Although the cleaning is time consuming in both processes, using the microfluidic system, residual loss of

SPIONS was achieved and the process was performed autonomously, contrarily to the manual cleaning. It is important to notice the relevance of this automatic process, once high quantities of MN are typically lost during manual cleaning. Moreover, repeating the cleaning process a second time using the same microfluidic system, no trace of NH_4OH was detected in the cleaning solution with SPIONS, which indicates that two series of the same microfluidic channels design are enough to clean properly SPIONS. The system is also useful for related coated or functionalized SPIONS or other MN. In fact, the microfluidic system was also tested for the cleaning and separation of silica-coated SPIONS [35], adapting the magnetic force applied, with cleaning efficiencies similar to the ones previously presented.

4 Conclusions

A microfluidic system was designed, fabricated and tested for the autonomous, continuous and effective cleaning and separation of MN, as an alternative solution to the time consuming and inefficient manual cleaning. A theoretical study was firstly performed to optimize the geometrical configuration of the microfluidic channel and the experimental conditions, taking advantage of existing laminar flow at this scale. After the proper fabrication and functionalization of the PDMS microfluidic system, it was tested for the cleaning and separation of synthesized SPIONS using NH_4OH as catalyst. Water was used as cleaning solution and a permanent magnet was properly located near the microchannel to apply the magnetic force in order to guaranty the deflection of the MN from the synthesis solution to the cleaning solution. Gas chromatography results demonstrated the potential of the microfluidic technology with cleaning efficiency as high as 99.7 % adapting properly the fluid flow rates at the inlets of the optimized microfluidic system. This result is superior to the manual cleaning that achieved a value

of about 94.3 % after six successive cleaning. Although the cleaning is time consuming in both processes, the microfluidic system shows residual loss of SPIONS and the process is performed autonomously. Moreover, the response time can be reduced increasing the flow rate and adapting experimental parameters, including magnetic force and microfluidic system configuration, accordingly. These results are promising for the fabrication of MN cleaning microfluidic platforms.

Acknowledgements

The authors thank the FCT - Fundação para a Ciência e Tecnologia - for financial support under framework of the Strategic Funding UID/FIS/04650/2013, project PTDC/EEI-SII/5582/2014 and project UID/EEA/04436/2013 by FEDER funds through the COMPETE 2020 – Programa Operacional Competitividade e Internacionalização (POCI) with the reference project POCI-01-0145-FEDER-006941. Funds provided by FCT through the Chemistry Research Centre of the University of Minho (Ref. UID/QUI/00686/2013 and UID/QUI/0686/2016) and in the framework of EuroNanoMed 2016 call, Project LungChek ENMed/0049/2016 are also gratefully acknowledged. VFC also thanks the FCT for the grant SFRH/BPD/98109/2013. Finally, the authors acknowledge funding by the Spanish Ministry of Economy and Competitiveness (MINECO) through the project MAT2016-76039-C4-3-R (AEI/FEDER, UE) and from the Basque Government Industry Department under the ELKARTEK program.

References

[1] Q. Du, T. Ma, C. Fu, T. Liu, Z. Huang, J. Ren, et al., Encapsulating Ionic Liquid and Fe3O4 Nanoparticles in Gelatin Microcapsules as Microwave Susceptible Agent for MR Imaging-guided Tumor Thermotherapy, ACS Applied Materials & Interfaces, 7(2015) 13612-9.
[2] Y. Zhou, Q. Xie, Hyaluronic acid-coated magnetic nanoparticles-based selective collection and detection of leukemia cells with quartz crystal microbalance, Sensors and Actuators B: Chemical, 223(2016) 9-14.

[3] S. Jiang, K.Y. Win, S. Liu, C.P. Teng, Y. Zheng, M.-Y. Han, Surface-functionalized nanoparticles for biosensing and imaging-guided therapeutics, Nanoscale, 5(2013) 3127-48.
[4] J.H. Gao, H.W. Gu, B. Xu, Multifunctional Magnetic Nanoparticles: Design, Synthesis, and Biomedical Applications, Accounts Chem Res, 42(2009) 1097-107.
[5] Q.A. Pankhurst, J. Connolly, S.K. Jones, J. Dobson, Applications of magnetic nanoparticles in biomedicine, J Phys D-Appl Phys, 36(2003) R167-R81.
[6] P. Tartaj, M.D. Morales, S. Veintemillas-Verdaguer, T. Gonzalez-Carreno, C.J. Serna, The preparation of magnetic nanoparticles for applications in biomedicine, J Phys D-Appl Phys, 36(2003) R182-R97.
[7] T. Kokalj, E. Perez-Ruiz, J. Lammertyn, Building bio-assays with magnetic particles on a digital microfluidic platform, New Biotechnology, 32(2015) 485-503.
[8] V. Nandwana, S.-R. Ryoo, S. Kanthala, M. De, S.S. Chou, P.V. Prasad, et al., Engineered Theranostic Magnetic Nanostructures: Role of Composition and Surface Coating on Magnetic Resonance Imaging Contrast and Thermal Activation, ACS Applied Materials & Interfaces, 8(2016) 6953-61.
[9] J. Liang, Y. Wu, C. Liu, Y.-C. Cao, J.A. Liu, Y. Lin, Preparation of high stable core/shell magnetic nanoparticles and application in Bacillus thuringiensis Cry1Ac proteins detection, Sensors and Actuators B: Chemical, 241(2017) 758-64.
[10] M.K. Jaiswal, M. De, S.S. Chou, S. Vasavada, R. Bleher, P.V. Prasad, et al., Thermoresponsive Magnetic Hydrogels as Theranostic Nanoconstructs, ACS Applied Materials & Interfaces, 6(2014) 6237-47.
[11] R. Hao, R.J. Xing, Z.C. Xu, Y.L. Hou, S. Gao, S.H. Sun, Synthesis, Functionalization, and Biomedical Applications of Multifunctional Magnetic Nanoparticles, Adv Mater, 22(2010) 2729-42.
[12] W. Wu, C.Z. Jiang, V.A.L. Roy, Designed synthesis and surface engineering strategies of magnetic iron oxide nanoparticles for biomedical applications, Nanoscale, 8(2016) 19421-74.
[13] M.C. Mascolo, Y. Pei, T.A. Ring, Room Temperature Co-Precipitation Synthesis of Magnetite Nanoparticles in a Large pH Window with Different Bases, Materials, 6(2013) 5549-67.
[14] J. Sun, S. Zhou, P. Hou, Y. Yang, J. Weng, X. Li, et al., Synthesis and characterization of biocompatible Fe3O4 nanoparticles, J Biomed Mater Res Part A, 80A(2007) 333-41.
[15] L. Zhang, W.-F. Dong, H.-B. Sun, Multifunctional superparamagnetic iron oxide nanoparticles: design, synthesis and biomedical photonic applications, Nanoscale, 5(2013) 7664-84.
[16] N. Pamme, Magnetism and microfluidics, Lab Chip, 6(2006) 24-38.
[17] H. Tsutsui, C.M. Ho, Cell separation by non-inertial force fields in microfluidic systems, Mech Res Commun, 36(2009) 92-103.
[18] S. Belaid, S. Laurent, M. Vermeech, L. Vander Elst, D. Perez-Morga, R.N. Muller, A new approach to follow the formation of iron oxide nanoparticles synthesized by thermal decomposition, Nanotechnology, 24(2013).
[19] P. Sajeesh, A.K. Sen, Particle separation and sorting in microfluidic devices: a review, Microfluid Nanofluid, 17(2014) 1-52.
[20] J. Shen, H. Liu, C. Mu, J. Wolfram, W. Zhang, H.-C. Kim, et al., Multi-step encapsulation of chemotherapy and gene silencing agents in functionalized mesoporous silica nanoparticles, Nanoscale, 9(2017) 5329-41.
[21] X. Han, Y. Feng, Q. Cao, L. Li, Three-dimensional analysis and enhancement of continuous magnetic separation of particles in microfluidics, Microfluid Nanofluid, 18(2015) 1209-20.
[22] Y. Chen, Y. Xianyu, J. Sun, Y. Niu, Y. Wang, X. Jiang, One-step detection of pathogens and cancer biomarkers by the naked eye based on aggregation of immunomagnetic beads, Nanoscale, 8(2016) 1100-7.
[23] X. Yao, X. Niu, K. Ma, P. Huang, J. Grothe, S. Kaskel, et al., Graphene Quantum Dots-Capped Magnetic Mesoporous Silica Nanoparticles as a Multifunctional Platform for Controlled

Drug Delivery, Magnetic Hyperthermia, and Photothermal Therapy, Small, 13(2017) 1602225-n/a.
[24] N. Xia, T.P. Hunt, B.T. Mayers, E. Alsberg, G.M. Whitesides, R.M. Westervelt, et al., Combined microfluidic-micromagnetic separation of living cells in continuous flow, Biomed Microdevices, 8(2006) 299-308.
[25] A. Lenshof, T. Laurell, Continuous separation of cells and particles in microfluidic systems, Chem Soc Rev, 39(2010) 1203-17.
[26] N. Pamme, Continuous flow separations in microfluidic devices, Lab Chip, 7(2007) 1644-59.
[27] V.F. Cardoso, L. Rebouta, S. Lanceros-Méndez, G. Minas, Transparent P(VDF-TrFE) transducer-based acoustic streaming for microfluidic applications, 17th International Conference on Miniaturized Systems for Chemistry and Life Sciences, MicroTAS 20132013, pp. 1884-6.
[28] J.J. Lai, K.E. Nelson, M.A. Nash, A.S. Hoffman, P. Yager, P.S. Stayton, Dynamic bioprocessing and microfluidic transport control with smart magnetic nanoparticles in laminar-flow devices, Lab Chip, 9(2009) 1997-2002.
[29] S. Naher, D. Orpen, D. Brabazon, C.R. Poulsen, M.M. Morshed, Effect of micro-channel geometry on fluid flow and mixing, Simul Model Pract Theory, 19(2011) 1088-95.
[30] D. Mark, S. Haeberle, G. Roth, F. von Stetten, R. Zengerle, Microfluidic lab-on-a-chip platforms: requirements, characteristics and applications, Chem Soc Rev, 39(2010) 1153-82.
[31] X. Xu, Z. Li, A. Nehorai, Finite element simulations of hydrodynamic trapping in microfluidic particle-trap array systems, Biomicrofluidics, 7(2013).
[32] Y. Ma, C.-P. Sun, M. Fields, Y. Li, D.A. Haake, B.M. Churchill, et al., An unsteady microfluidic T-form mixer perturbed by hydrodynamic pressure, Journal of Micromechanics and Microengineering, 18(2008).
[33] L. Capretto, W. Cheng, M. Hill, X. Zhang, Micromixing Within Microfluidic Devices, in: B.C. Lin (Ed.) Microfluidics: Technologies and Applications2011, pp. 27-68.
[34] V.C. Pinto, P.J. Sousa, V.F. Cardoso, G. Minas, Optimized SU-8 Processing for Low-Cost Microstructures Fabrication without Cleanroom Facilities, Micromachines, 5(2014) 738-55.
[35] V.F. Cardoso, S. Irusta, N. Navascues, S. Lanceros-Mendez, Comparative study of sol–gel methods for the facile synthesis of tailored magnetic silica spheres, Materials Research Express, 3(2016) 075402.